

Quantum dynamics of $H^+ + CO$ collisions

F. George D. Xavier* and Sanjay Kumar

Department of Chemistry, Indian Institute of Technology Madras, Chennai, India

(Received 17 October 2010; published 18 April 2011)

The vibrational mode-selective scattering properties have been computed for the $H^+ + CO$ system at two experimentally reported collision energies, $E_{c.m.} = 9.5$ eV and $E_{c.m.} = 28.96$ eV, for elastic, inelastic, and charge-transfer channels, using the vibrational close-coupling rotationally infinite-order sudden approximation (VCC-RIOS) scheme, making use of the *ab initio* potentials of the ground-state (GS) and the first-excited-state (ES) potential energy surfaces (PESs) of the bound HCO^+ molecule computed at the multireference configuration interaction (MRCI) level of accuracy and using the *cc-pVTZ* basis set in Jacobi coordinates (R, r, γ) . The vibronic couplings used as input in computing the scattering quantities were computed and compared with previously reported couplings to give a fair idea about the extent of deviation from the present work. The scattering quantities are compared with the available experimental results and the computed data are found to match the experimental results even though there are noteworthy disagreements.

DOI: [10.1103/PhysRevA.83.042709](https://doi.org/10.1103/PhysRevA.83.042709)

PACS number(s): 34.70.+e, 34.50.Ez

I. INTRODUCTION

Proton-molecule collisions occur dominantly in interstellar medium leading to the formation of many bound protonated molecular ions like H_3^+ , N_2H^+ , HCO^+ , HO^+ , HCS^+ , HO_2^+ , etc. [1,2]. They are proposed to be formed through various elastic-inelastic or charge-transfer processes. As a result, the proton-molecule interaction has been the subject of many experimental and theoretical studies, and a wealth of varied experimental information on inelastic vibrational excitation (IVE) and vibrational charge-transfer (VCT) excitation has become available over the years using the molecular beam and the proton energy-loss spectroscopy techniques [3–9]. The focus has been on collision energies in the range 0–30 eV where extensive vibrational-rotational excitations of the target molecules occur along with possible VCT processes. There have been several experimental studies on proton collisions with diatomic and polyatomic targets such as H_2 , N_2 , O_2 , CO , NO , HF , HCl , CH_4 , SF_6 , etc., leading to an interesting finding of marked selectivity in vibrational excitations of apparently similar molecules. The dynamics of complex formation via translation-to-vibration energy exchange and types of resonances exhibited by the complex have also been studied [10].

It is worth pointing out here that the $HCO^+ + CO$ is also an important astrophysical system ever since it was proposed [11] that the bound molecular HCO^+ and HO^+ ions could be the likely source of an unidentified microwave line observed [12] from interstellar space. The experimental observation of the rotational spectrum of HCO^+ in the laboratory using the microwave technique [13] confirmed its presence in interstellar medium, and it was the first polyatomic ion to be detected in outer space. Experiments [5] were performed on N_2 , CO , and NO in the energy range $E_{lab} = 30$ –80 eV in the small scattering angular region around 0° as well as in the rainbow region around 9° , predicting low-vibrational inelasticity in all of them. In the later experiments [6], which included O_2 in

addition to the above species, vibrationally resolved scattering quantities such as probability ($P_{0 \rightarrow v}$), mean energy transfer ($\Delta \bar{E}_{vib}$), and so forth were obtained at $E_{lab} = 10$ eV. The endoergicity between the charge-transfer and the inelastic processes in the proton impact on CO at $E_{c.m.} = 28.96$ eV was experimentally measured and reported [9] along with measurements of the differential cross section (DCS) summed over vibrational states for the charge-transfer process.

There have been quite a lot of *ab initio* calculations performed in the past [14–23] to characterize the equilibrium structure of HCO^+ and to determine the proton affinity of CO . The knowledge of high-level *ab initio* potential energy surfaces (PESs) of different electronic states and the interaction potential among them is required to undertake multistate dynamics calculations and they are available for $H^+ + H_2$ [24–26], $H^+ + O_2$ [27–32], $H^+ + N_2$ [33,34], and $H^+ + NO$ [35]. But for $H^+ + CO$ [23,36–42], some limited amount of work has been done in the past especially computing the PES of the ground state (GS) alone followed by the dynamics study. Until recently, there has been a lack of diabatic PESs of the GS and the first excited state (ES) and we have addressed this lack by undertaking the computation of these PESs, which are reported elsewhere [43].

In this article, we report the scattering dynamics for the experimentally observed elastic-inelastic, $H^+ + CO(X^1\Sigma^+, v=0) \rightarrow H^+ + CO(X^1\Sigma^+, v \neq 0)$, and charge-transfer (electron capture), $H^+ + CO(X^1\Sigma^+, v=0) \rightarrow H(^2S) + CO^+(X^2\Sigma^+, v')$, processes, undertaken based on the computed two-state diabatic PESs and their interaction potential reported earlier [43]. This paper is organized as follows. In Sec. II we discuss the computational details and in Sec. III we present the details of computed scattering quantities, followed by a summary in Sec. IV.

II. THE COMPUTATIONAL DETAILS

Though carrying out time-independent quantum dynamical calculations with a full close-coupling approach is computationally expensive, it is possible to make a few reasonable approximations to decouple the angular momenta, keeping the

*george.iitm@gmail.com; Institute of Chemistry, Hebrew University, Jerusalem, Israel.

magnitude of collision energy of the projectile in mind, thus making the computations a practically achievable task. Since the collision energy is at relatively high range, $E_{c.m.} = 9.5$ eV and $E_{c.m.} = 28.96$ eV, we can make two valid approximations: (i) freezing of the rotational motion of the target molecule and (ii) neglecting the discrete rotational states of the target molecule. These two approximations form the basis of the vibrational close-coupling rotationally infinite-order sudden approximation (VCC-RIOSAs) decoupling scheme for effective numerical implementation. The first assumption is valid when the kinetic energy (KE) of the projectile is comparatively

high and the rotational motion of the target molecule is low and the second one is valid when the KE is far higher than the energy gap of discrete rotational states of the target. In our calculation we assume implicitly that both of these conditions are met and hence invoking the VCC-RIOSAs scheme is fully justified. The history of various quantum sudden approximations is reviewed elsewhere [44–49].

In the diabatic representation, the two coupled nuclear Schrödinger equations in the Jacobi coordinates for the $A^+ + BC$ system can be written as

$$\left[-\frac{\hbar^2}{2\mu_{ABC}} \frac{\partial^2}{\partial R^2} - \frac{\hbar^2}{2\mu_{BC}} \frac{\partial^2}{\partial r^2} + \frac{\hbar^2}{2\mu_{ABC}} \frac{l(l+1)}{R^2} + \frac{\hbar^2}{2\mu_{BC}} \frac{j(j+1)}{r^2} + V_{11}^d(R,r;\gamma) + V_{BC}(r) - E \right] \times \psi_1(R,r;\gamma) + V_{12}^d(R,r;\gamma)\psi_2(R,r;\gamma) = 0, \quad (1a)$$

$$\left[-\frac{\hbar^2}{2\mu_{ABC}} \frac{\partial^2}{\partial R^2} - \frac{\hbar^2}{2\mu_{BC}} \frac{\partial^2}{\partial r^2} + \frac{\hbar^2}{2\mu_{ABC}} \frac{l(l+1)}{R^2} + \frac{\hbar^2}{2\mu_{BC}} \frac{j(j+1)}{r^2} + V_{22}^d(R,r;\gamma) + V_{BC^+}(r) - E \right] \times \psi_2(R,r;\gamma) + V_{21}^d(R,r;\gamma)\psi_1(R,r;\gamma) = 0, \quad (1b)$$

where μ_{ABC} is the atom-molecule reduced mass, μ_{BC} is the reduced mass of the diatom, $l(l+1)\hbar^2$ is the orbital angular momentum of the atom A^+ relative to the molecule BC, $j(j+1)\hbar^2$ is the rotational angular momentum of the diatom BC, V_{BC} is the diatomic potential of BC system, and V_{BC^+} is the diatomic potential of the BC^+ system. These coupled equations can be transformed into a set of vibrational close-coupling equations and the number of such equations depends upon the product of the number of vibrational states of the CO and CO^+ involved, respectively. In order to have converged cross sections for states up to $v(v') = 5$ in the range of the experimental collision energies $E_{c.m.} = 9.5$ – 28.96 eV, 10 vibrational energy levels of the target diatom CO correlating to the ground electronic diabatic state (V_{11}^d) and 10 vibrational levels of the CO^+ system correlating to the first excited electronic diabatic state (V_{22}^d) were included in the vibrational close-coupling calculations. The coupled-channel equations were solved by the sixth-order Numerov method for 13 equally spaced orientations with γ values between 0° and 180° at the interval of 15° for each partial wave (l) using Le Roy's code [50]. $\gamma = 0^\circ$ describes the H^+ approach toward the O end of CO in the collinear geometry. For elastic $0 \rightarrow 0$ excitations at $E_{c.m.} = 28.96$ eV, the maximum number of partial waves (l_{max}) was 1200. The vibrational wave functions and the corresponding eigenvalues (required to compute vibronic coupling) were determined by solving the nuclear Schrödinger equation of the CO and the CO^+ diatoms. The vibronic couplings $V(R;\gamma)$ were computed for each value of γ as a function of R over a fine mesh of r by numerical integration.

Since the sudden S -matrix elements in the ion-molecule systems are known to show a strong γ dependence particularly at small l , the sudden (rotationally summed) T -matrix ele-

ments were expanded in terms of Legendre polynomials [49] at each l as

$$T_{vv'}^{jl}(\gamma) = \sum_{\lambda} A_{\lambda}^l(jv \rightarrow v') P_{\lambda}(\cos \gamma). \quad (2)$$

Using the orthogonality of the Legendre polynomials, the expansion coefficients A_{λ}^l were determined by a set of linear equations as follows:

$$\sum_{\lambda=0}^{N^*} A_{\lambda}^l(jv \rightarrow v') \sum_{i=1}^N P_{\lambda}(\cos \gamma_i) P_{\lambda'}(\cos \gamma_i) = \sum_{i=1}^N T_{vv'}^{jl}(\gamma_i) P_{\lambda'}(\cos \gamma_i). \quad (3)$$

In the present case $\lambda, \lambda' = 0, 1, 2, \dots, N^*$; $N^* \leq N$; $\gamma_1 = 0^\circ$; $\gamma_N = 180^\circ$; and $N = 13$. The state-to-state DCSs were obtained as

$$\frac{d\sigma}{d\omega}(jv \rightarrow v') = \sum_{\lambda} (2\lambda + 1)^{-1} \frac{d\sigma^{\lambda}}{d\omega}(jv \rightarrow v'), \quad (4)$$

where

$$\frac{d\sigma^{\lambda}}{d\omega}(jv \rightarrow v') = \left(\frac{1}{4k_{jv}^2} \right) \left| \sum_l (2l + 1) P_l(\cos \theta_{c.m.}) A_{\lambda}^l(jv \rightarrow v') \right|^2. \quad (5)$$

Here, $\theta_{c.m.}$ is the scattering angle in center of mass (c.m.) frame of reference and k_{jv}^2 denotes the usual wave vector selected within the infinite-order sudden approximation. All the calculations were performed for a rotational quantum

number $j = 0$ of the target diatom. Similarly, integral cross sections were obtained as

$$\sigma(jv \rightarrow v') = \sum_{\lambda} (2\lambda + 1)^{-1} \sigma^{\lambda}(jv \rightarrow v'), \quad (6)$$

where

$$\sigma^{\lambda}(jv \rightarrow v') = \left(\frac{\pi}{k_{jv}^2} \right) \sum_l (2l + 1) |A_{\lambda}^l(jv \rightarrow v')|^2. \quad (7)$$

One can also obtain the orientation-dependent integral cross section as

$$\sigma(jv \rightarrow v'; \gamma) = \left(\frac{\pi}{k_{jv}^2} \right) \sum_l (2l + 1) |T_{vv'}^{jl}(\gamma)|^2, \quad (8)$$

from which one further obtains a useful angle-dependent quantity called opacity as

$$\sigma^l(jv \rightarrow v'; \gamma) = \left(\frac{\pi}{k_{jv}^2} \right) (2l + 1) |T_{vv'}^{jl}(\gamma)|^2. \quad (9)$$

All the above computed quantities can help us, as we shall see below, to further characterize the behavior of the inelastic and charge-transfer scattering processes.

III. RESULTS AND DISCUSSIONS

We compare the computed dynamical quantities with those of experiments at $E_{c.m.} = 9.5$ eV [6] and $E_{c.m.} = 28.96$ eV [5,9]. The state-to-state experimental data are available only for the elastic-inelastic process at $E_{c.m.} = 9.5$ eV and $E_{c.m.} = 28.96$ eV. They are reported in terms of laboratory frame of reference (lab) in the literature and are converted to c.m. frame for easy comparison with theoretical results through the relation

$$\sin \theta_{c.m.} = \frac{\sin \theta_{lab}}{m_2} \left(m_1 \cos \theta_{lab} + \sqrt{m_2^2 - m_1^2 \sin^2 \theta_{lab}} \right), \quad (10)$$

$$E_{c.m.} = E_{lab} \left(\frac{m}{m + M} \right),$$

where θ is the scattering angle; m_1 , m_2 , and m_3 are the masses of the atoms in the triatomic system; and m and M are the masses of the projectile and the target molecule of the collision system. $E_{c.m.}$ & E_{lab} are the collision energies in their respective frame of reference. Niedner-Schatteburg and Toennies [9] had reported the total DCS for the charge-transfer channel at $E_{c.m.} = 28.96$ eV. Before discussing below the computed quantities one by one, we have to have an idea about the vibronic couplings which govern the transitions between the two electronic states and are used as input data to compute scattering quantities such as cross sections, mean energy transfer, etc.

A. Vibronic coupling

The vibronic coupling in the diabatic representation is calculated using the integral (sum over r) $V(R; \gamma) = \langle \chi_{CO}(r) | V_{12}(R, r, \gamma) | \chi_{CO^+}(r) \rangle$, where $V_{12}(R, r, \gamma)$ is the γ -dependent interaction potential between the GS and the first ES state obtained from the *ab initio* calculation reported earlier [43] and $\chi_{CO}(r)$ and $\chi_{CO^+}(r)$ are the diatomic wave

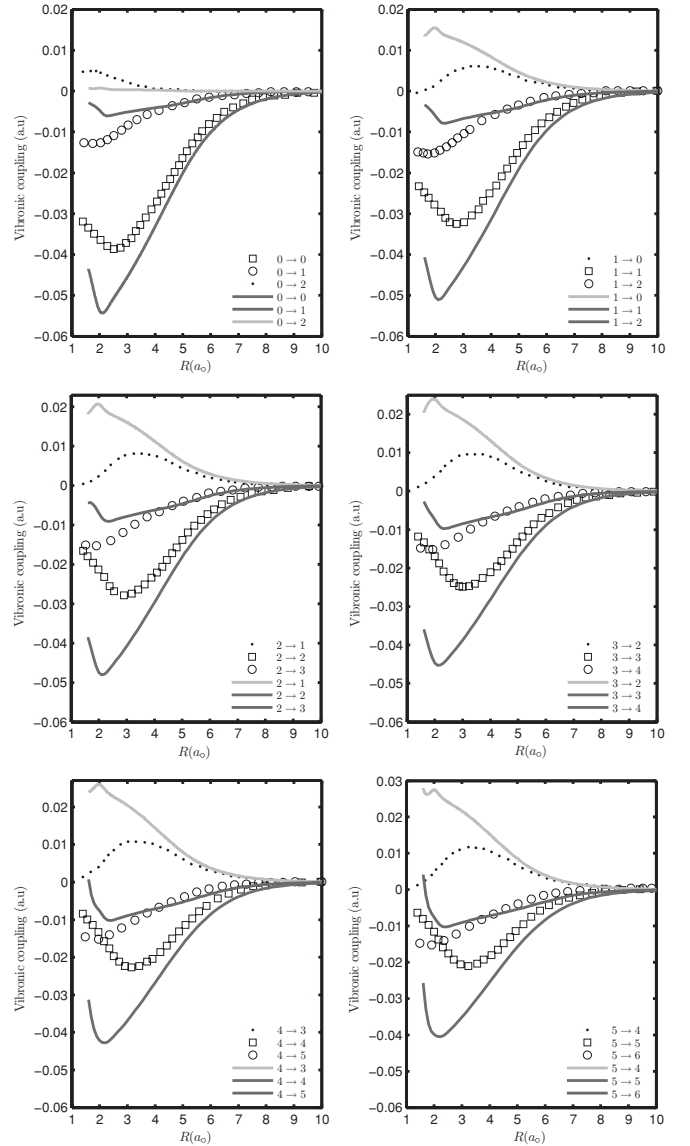


FIG. 1. (Color online) Vibronic coupling for $\gamma = 90^\circ$ as a function of R connecting the states $v = 0-5$ with the states $v' = v$ and $v \pm 1$ along with the results from the earlier work [39].

functions as a function of bond distance for a given eigenstate, with 10 such states included in the computation and $V(R; \gamma)$ is the γ -dependent vibronic coupling. The computed vibronic couplings are shown and compared with earlier work [39] in Fig. 1. Those with larger $|\Delta v|$ are significantly smaller and hence are not shown. As we can see, the deviation of coupling between the present work and the earlier one [39] is highly marked in the interaction region ($R = 1.8 \leftrightarrow 5$; $r = 1.8 \leftrightarrow 2.5$) rather than in the asymptotic region where there is a relatively good agreement. The strength of coupling follows the order: $v = 1-5 \rightarrow v' = v > v = 1-5 \rightarrow v' = v-1 > v = 1-5 \rightarrow v' = v+1$ when $v \neq 0$. When $v = 0$ the order is $v = 0 \rightarrow v' = 0 > v = 0 \rightarrow v' = 1 > v = 0 \rightarrow v' = 2$. This prediction seems to be little different from the previous work where the intensities of the transitions $v = 0-5 \rightarrow v' = v-1 \sim v = 0-5 \rightarrow v' = v+1$ are almost of the same order of magnitude. The relative magnitudes of

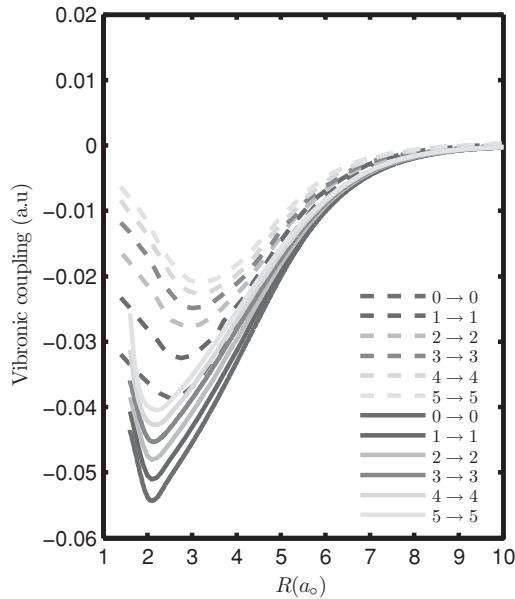


FIG. 2. (Color online) Vibronic coupling for diagonal transitions in the present and earlier work.

the diagonal ($v = 0 - 5 \rightarrow v' = v$) transitions are shown as a group of solid lines along with the dashed lines denoting the earlier work in Fig. 2. The discrepancies stated above seem to arise from the fact that the CO and CO^+ ground state potentials used in the previous work were taken from some earlier work [51,52] which was based on the semiclassical approach of the Rydberg-Klein-Rees (RKR) method and an extended Hartree-Fock method with the help of the RKR method. In this work, the diatomic potentials were calculated using the $cc\text{-}p\text{VTZ}$ basis set [53] and a multireference configuration interaction (MRCI) level of sophistication [54–60] with precise numerical convergence. The numerical difference exists between them as can be found from the dissociation energies of CO in the ground state, which are roughly 10.8 eV (this work) and 11.4 eV (previous work). Also the computed first ES potential for HCO^+ , particularly for $\gamma = 180^\circ$, in this work [43] differs greatly from what was reported [39,40] because of conical intersection with the third electronic state and this makes the associated diabatic coupling potential differ a lot numerically. All these factors are responsible for the discrepancies and the accuracy of vibronic coupling can be verified only from the computed scattering quantities and its closeness with the experimental results.

B. Opacity function

The expression to compute opacity function for elastic-inelastic as well as charge-transfer processes is given in Eq. (9) in Sec. II. We have assumed $j = 0$ throughout the calculation, implying that the target molecule does not rotate during the collision. It is defined as the relative probability that a given process occurs from the initial vibrational state to the final state as a function of the impact parameter, which is related to each contributing l value through the relation $pb = (l + \frac{1}{2})$, where p is the momentum of the projectile and b is the impact parameter. We present in Fig. 3 the computed opacities as a function of

the number of partial waves (l) for elastic-inelastic and charge-transfer processes at $E_{c.m.} = 28.96$ eV alone. But whatever is stated at this energy will mostly hold good at $E_{c.m.} = 9.5$ eV. The l_{max} is found to be dependent on the collision energy, the type of process, and the angular approach (angle between incoming proton and internuclear axis of the target molecule) of the projectile. Usually elastic-inelastic processes requires more number of partial waves before attaining the maximum probability than the charge-transfer processes. In the $\text{H}^+ + \text{CO}$ system, $l_{max} \sim 800(400)$ at $E_{c.m.} = 9.5$ eV and $l_{max} \sim 1200(800)$ at $E_{c.m.} = 28.96$ eV for the elastic-inelastic and charge-transfer processes, respectively. For any process to occur with reasonable probability, a sufficient number of contributing partial waves are needed in order to have a sufficiently large impact parameter. Beyond l_{max} , the opacity falls to practically zero, implying that the probability of any process to occur is virtually nil whatever the number of contributing partial waves. Thus it is clear that maximum opacity occurs only at a specific impact parameter value (not over a range of values). The first row in Fig. 3 refers to the opacity at $\gamma = 90^\circ$ and the order of opacity as measured from peak heights is given as $0 \rightarrow 0 > 0 \rightarrow 1 > 0 \rightarrow 2$ for the elastic-inelastic channel, with $0 \rightarrow 1$ and $0 \rightarrow 2$ transitions being multiplied by a factor of 10 for better clarity and the same order is followed for the charge-transfer channel too. This ordering also holds good for other angles at this collision energy as well as at $E_{c.m.} = 9.5$ eV (not shown). The elastic collision is the strongest followed by inelastic and charge-transfer collisions. Since the angular dependency plays a crucial role in the relative probability (known as the steric effect) of a particular transition, we show in the second row of Fig. 3 the influence of γ on the elastic channel, $0 \rightarrow v = 0$, as well as on the charge-transfer channel, $0 \rightarrow v' = 0$. For the elastic process, the ordering determined from the maximum peak heights (the point of highest impact parameter) is $180^\circ > 90^\circ > 0^\circ$ while for the charge-transfer process the order is $90^\circ > 180^\circ > 0^\circ$.

C. Cross section

The cross section is an important quantity in the scattering theory as it provides us a way to identify short-lived states, if any, formed during collisions and it can be calculated through the relation given in Eq. (4) in Sec. II. The computation was done at two collision energies, $E_{c.m.} = 9.5$ eV and $E_{c.m.} = 28.96$ eV, and we report only a few essential results, especially those supported by experimental evidence. We sum up the state-to-state DCS up to 10 vibrational states to give the total DCS which deserves special attention. The computed data contain considerable undulatory structures due to various types of quantum interferences and fast oscillations effects, and the experimental results are free of those features. Hence we smoothed the computed data using the spline technique to avoid irregularities (not numerical errors) for better comparison and only those smoothed data are shown in Fig. 4 along with experimental results [5,9] for both the channels.

The comparison of the cross section at 9.5 and 28.96 eV reveals that its magnitude decreases as $\theta_{c.m.}$ increases and the decrease is too drastic in the case of the latter. This is

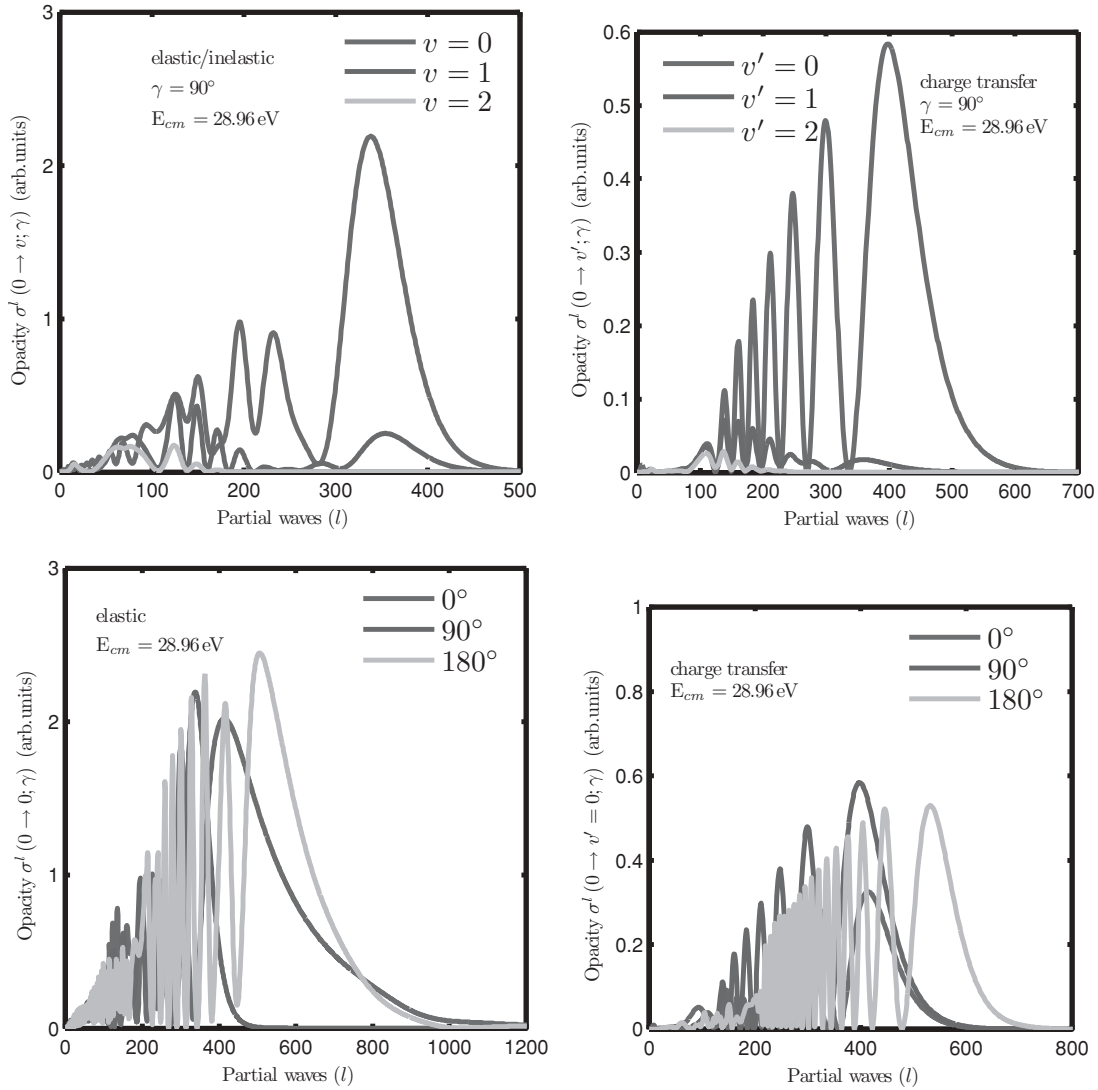


FIG. 3. (Color online) Opacity function as a function of partial waves (l) in units of \hbar , with actual opacities multiplied by a factor 10 for inelastic transitions for magnification purposes only in the first plot of the top row.

quite expected since the experimental results are also exhibit a similar trend of angular dependency. At both energies, the cross sections do not vary appreciably as a function of $\theta_{c.m.}$ for a given channel in the small angular regions and the variation becomes significant once $\theta_{c.m.}$ becomes high. The cross section gap between the two channels remains more

or less the same at both energies except when $\theta_{c.m.} \rightarrow 0^\circ$, where the gap explodes to a large value. At $\theta_{c.m.} = 0^\circ$, the cross section is higher for the elastic-inelastic channel than for the charge-transfer channel and it is higher at 28.96 eV than at 9.5 eV. The comparison is made between theory and experiments [9] at 28.96 eV for the total DCS and the

TABLE I. Transition probabilities compared with experiment [6].

$P_{0 \rightarrow v}$ at 9.5 eV									
$\theta_{c.m.}$	Elastic/inelastic						Charge transfer		
	Expt.			Theory			Theory		
	$v = 0$	1	2	0	1	2	$v' = 0$	1	2
5.2	0.97	0.03		0.96	0.03	0.01	0.96	0.03	3×10^{-3}
10.4	0.88	0.09	0.03	0.91	0.06	0.02	0.90	0.06	0.01
15.5	0.83	0.12	0.05	0.82	0.10	0.04	0.77	0.09	0.04
20.7	0.71	0.22	0.07	0.80	0.13	0.04	0.80	0.10	0.04

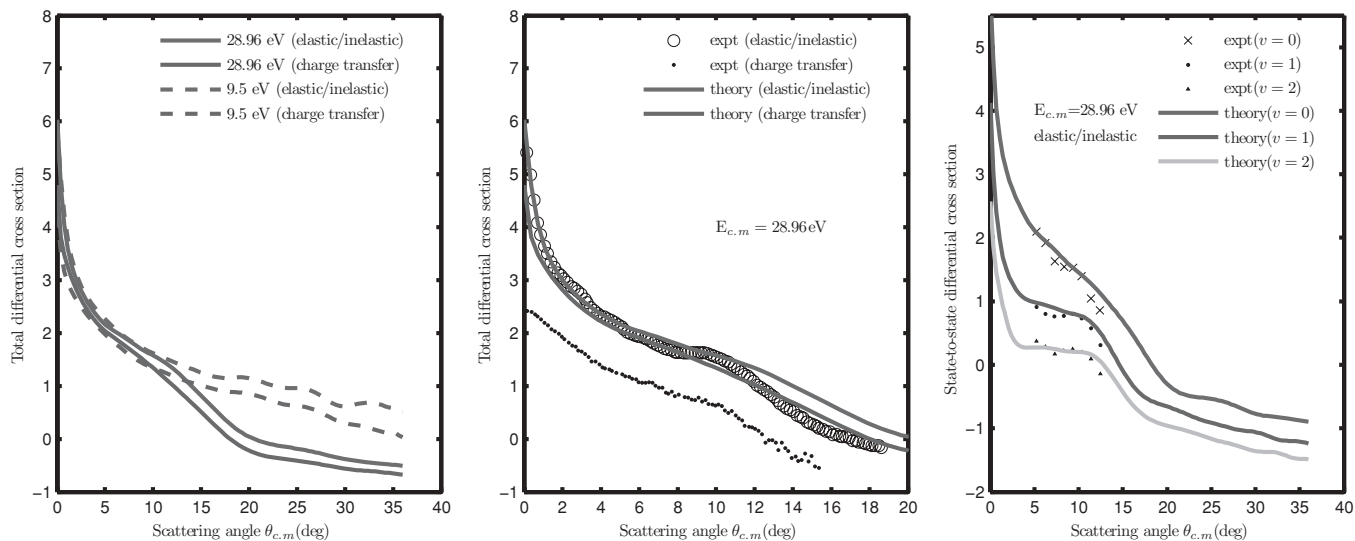


FIG. 4. (Color online) The computed cross sections and their comparison with experimental results [5,9] as a function of $\theta_{c.m.}$ at two collision energies.

experimental data (not absolute) are shifted by a fixed amount relative to theory at the datum point of $\theta_{c.m.} = 9.38^\circ$ which happens to be the point of rainbow maxima in the experimental data. The normalized experimental data and computed data agree well for the elastic-inelastic process in the small $\theta_{c.m.}$ and theory overestimates the experiment at higher $\theta_{c.m.}$ and yet the agreement seems to be encouraging for all practical purposes. Our results also predict the rainbow maximum around $\theta_{c.m.} \sim 10^\circ$, which is less intense and broad, compared to the prediction by the experiment, and this kind of maximum is absent at 9.5 eV. This sudden rise in the DCS is an indication of the existence of a short-lived species formed during the collision at a given collision energy. Unfortunately, there is huge numerical disagreement between the present work and the experiment with respect to the charge-transfer process. This is because the process is endoergic by 0.05 eV as predicted by this work, a value roughly 8 times smaller than the value (~ 0.4 eV) predicted by the experiment. This clearly suggests that theory predicts less endoergicity, and hence more probability of the process to occur, thus causing the difference in cross section between the two processes to be small, unlike in the experiments where a high endoergic value makes the charge-transfer process less probable, leading to the large difference in the cross section. In other words, theory overestimates the charge-transfer process while the experiments underestimate it. The accuracy of PESs is fully justified by comparing the computed molecular properties of HCO^+ with the experimental data in our earlier paper [43] and we suggest either repeating the experiments with more accurate procedures for the charge-transfer channel or carrying out the dynamics using four-state PESs assuming the insufficiency of two-state PESs.

The computed smoothed state-to-state cross sections for the first three vibrational states show a good agreement after the experimental data [5] are shifted by a fixed amount at the rainbow maximum of the $v = 0$ state lying at $\theta_{c.m.} = 9.36^\circ$. Though the experimental data are available only for a small range, the computed data are shown in

the extended region too. The cross section for the elastic transition ($0 \rightarrow v = 0$) is the highest among all excitations. Our data explain well the variation of experimental cross section as a function of $\theta_{c.m.}$ in the given experimental range.

D. Transition probability

The detailed behavior of the individual probabilities as a function of the scattering angle is also a good tool for further analysis of the performance of the present *ab initio* potential with respect to existing experimental values. It is nothing but

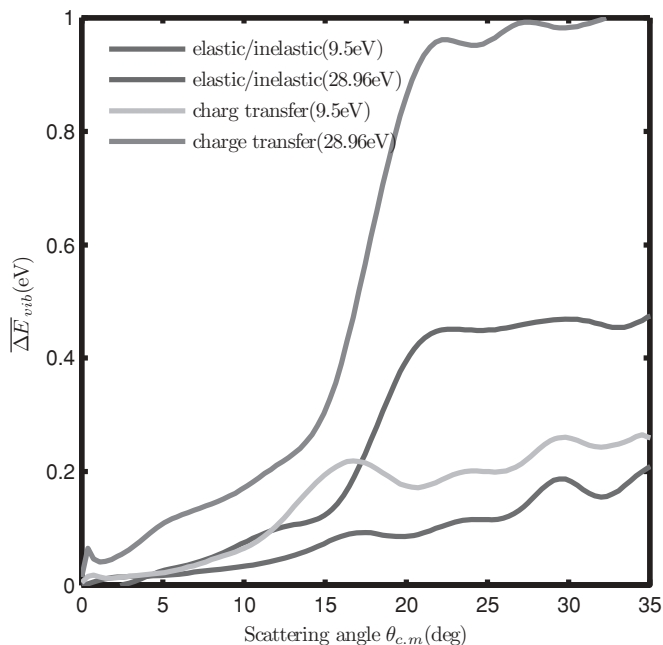


FIG. 5. (Color online) The computed energy transfer compared at two collision energies for the two processes.

TABLE II. Transition probabilities compared with experiment [5].

$P_{0 \rightarrow v}$ at 28.96 eV									
$\theta_{c.m.}$	Elastic/inelastic						Charge transfer		
	Expt.		Theory				Theory		
	$v = 0$	1	2	0	1	2	$v' = 0$	1	2
5.2	0.92	0.06	0.02	0.91	0.07	0.03	0.74	0.14	0.05
6.2	0.90	0.07	0.03	0.91	0.06	0.02	0.79	0.10	0.04
7.3	0.86	0.12	0.03	0.88	0.08	0.02	0.80	0.10	0.04
8.3	0.82	0.14	0.04	0.80	0.13	0.04	0.79	0.10	0.04
9.3	0.81	0.15	0.04	0.76	0.16	0.05	0.77	0.12	0.05
10.4	0.78	0.18	0.05	0.74	0.18	0.05	0.70	0.15	0.08
11.4	0.69	0.23	0.07	0.69	0.20	0.07	0.72	0.12	0.07
12.4	0.65	0.23	0.10	0.56	0.16	0.06	0.60	0.16	0.09

a ratio obtained by dividing the state-to-state cross section by the total cross section as shown in the formula below [61]:

$$P_{0 \rightarrow v}(\theta_{c.m.}) = \frac{\left. \frac{d\sigma}{d\omega}(0 \rightarrow v) \right|_{\theta_{c.m.}}}{\sum_{v \neq 0}^{\nu_{\max}} \left. \frac{d\sigma}{d\omega}(0 \rightarrow v) \right|_{\theta_{c.m.}}}, \quad (11)$$

where $\nu_{\max} = 10$. In Table I the computed values and the values from the experiment [6] at $E_{c.m.} = 9.5$ eV for both processes are shown. The elastic process, $0 \rightarrow v = 0$, is well predicted by the theory in terms of the numerical agreement as well as the angular dependency in the measured range of $\theta_{c.m.}$. The inelastic processes, $0 \rightarrow v = 1$, $0 \rightarrow v = 2$, and so forth, have all been well accounted for in terms of these two factors. The only difference is that the magnitudes of the probability for the inelastic processes are relatively very low compared to those of the elastic processes. The data from theory suggest the following order of magnitude, $0 \rightarrow 0 > 0 \rightarrow 1 > 0 \rightarrow 2 \dots$. The data on charge-transfer processes are given without experimental backup and hence one cannot study the suitability of the two-state model. The $0 \rightarrow v' = 0$ process occurs with maximum probability, with magnitude comparable to that of the elastic process. This enhancement in the relative probability is due to easy accessibility of the first electronic state from the ground state of HCO⁺ through long-range Demkov coupling [62,63] during collision as the asymptotic endoergicity of the reaction, $H^+ + CO \rightarrow H + CO^+$, is very low, of the order of 10^{-2} eV, as compared to the experimental one, which is of the order of 10^{-1} eV. This is also obvious from the vibronic coupling studied earlier in Fig. 1 where the magnitude of the $CO(v = 0) \rightarrow CO^+(v' = 0)$ transition is the highest among the transitions considered and is higher than the previously reported work [39]. This suggests that this transition occurs readily. The probabilities of other transitions are less and follow the order $0 \rightarrow v' = 0 > 0 \rightarrow v' = 1 > 0 \rightarrow v' = 2$. In Table II, the computed values and the data from experiment [5] at $E_{c.m.} = 28.96$ eV are shown for first three states for selected angles. The data on the charge-transfer process are given without experimental data due to their unavailability. We can see a good agreement between theory and experiment for the

elastic transition numerically as well as in the trend of variation of probability in the given angular range. Yet, the magnitude seems to be little decreased relative to that at $E_{c.m.} = 9.5$ eV and can be reasoned out by the presence of a weak broad rainbow maximum in the total DCS and the state-selective DCS of elastic transition. This feature indicates the existence of a short-lived transient species which is responsible for the decrease in the probability of the elastic channel at this collision energy. As usual, the inelastic channels are less likely to occur but with enhanced relative probability in comparison with 9.5 eV, and the ordering of transitions in terms of their likelihood is as given at $E_{c.m.} = 9.5$ eV. The transition to a higher level increases very slowly with respect to $\theta_{c.m.}$. In the case of the charge-transfer process, the $0 \rightarrow v' = 0$ transition is dominant over others but its magnitude is comparatively less, thus pointing out that the transition is favored more at $E_{c.m.} = 9.5$ than at $E_{c.m.} = 28.96$ eV. This is in contradiction to the explanation given for the charge-transfer process at 9.5 eV. This diminished probability is explained on the basis of the enormous vibrational excitation of target molecules, followed by their decay (transition to ground state) through various means, thus making the electron-capturing process less probable. The other transition follows the same order as listed for 9.5 eV, but with enhanced probability

E. Mean energy transfer

Another way of examining the quality of the calculations is given by the estimation of the average energy transfer as a

TABLE III. Mean energy transfer compared with experiment [6].

$\overline{\Delta E}_{vib}$ at 9.5 eV			
$\theta_{c.m.}$	Elastic/inelastic		Charge transfer
	Expt.	Theory	Theory
5.2	0.008	0.020	0.022
10.4	0.040	0.040	0.072
15.5	0.058	0.068	0.208
20.7	0.095	0.090	0.172

TABLE IV. Mean energy transfer compared with experiment [5].

$\theta_{c.m.}$	$\overline{\Delta E}_{vib}$ at 28.96 eV		
	Elastic/inelastic		Charge transfer
	Expt.	Theory	Theory
5.2	0.026	0.044	0.155
6.2	0.031	0.044	0.132
7.3	0.048	0.053	0.140
8.3	0.058	0.092	0.141
9.3	0.061	0.103	0.134
10.3	0.073	0.090	0.180

function of the scattering angle $\theta_{c.m.}$ as defined below:

$$\overline{\Delta E}_{vib}(\theta_{c.m.}) = \sum_{v=0}^{v_{max}} P_{0 \rightarrow v}(\theta_{c.m.}) \Delta E(0 \rightarrow v). \quad (12)$$

It is just the sum over the product of the transition probability and the vibrational energy level spacings between CO and CO⁺. We have taken $v_{max} = 10$ and the energy level spacings are consistent with the Morse oscillator model of diatomic molecules. Thus the computed quantity along with the experimental results [6] are tabulated in Table III for the four angles at $E_{c.m.} = 9.5$ eV. The general trend is to increase with angle and to extrapolate to a finite small value such as $\theta_{c.m.} \sim 0^\circ$ and our computed values clearly follow this trend along with good numerical matching. At small $\theta_{c.m.}$ the computed values are a bit larger and this is due to the fact that the vibronic coupling is very strong in the interaction region for the elastic-inelastic channels. As for the charge-transfer process, we give only theoretical values which increase first and drop beyond $\theta_{c.m.} \sim 15^\circ$. Generally its values are higher than those of the elastic process, thus reflecting the amount of energy associated with the vibrational states of CO⁺. In Table IV we provide the values at $E_{c.m.} = 28.96$ eV for both the processes in the angular range of 5° – 10° . We can see the same trend of variation but with little overestimated values for the elastic-inelastic channel due to the higher collision energy, and the numerical agreement is satisfactory. In the charge-transfer process, the energy transfer is high compared to that at $E_{c.m.} = 9.5$ eV with a small irregular variation seen at large $\theta_{c.m.}$. We compare the energy transfer at the two

collision energies for the two processes in Table V and we can clearly see that the magnitudes are directly proportional to the collision energies. One remarkable feature seen is that there is a “sudden jump” (nothing to do with the incident collision energy) in the transfer of energy in the middle region of the scattering angle for both processes at $E_{c.m.} = 28.96$ eV before leveling off at higher angles and all four curves converge to zero at $\theta_{c.m.} \rightarrow 0^\circ$. The “sudden jump” feature seen at $E_{c.m.} = 28.96$ could be explained based on the accessibility of more numbers of vibrational states at this energy. It is true that target molecules are excited to higher vibrational states on impact with H⁺, transferring its KE into these vibrational energy levels.

F. Integral cross section

The integral cross section is defined as the sum over the state-to-state cross sections over a specified angular range (lower and upper). In Table V we have listed those values for the two channels at the two collision energies up to the state of $v(v') = 7$ and their sum. Unfortunately, there are no experimental results to be compared with the computed data for either channel at both the energies. The integral cross section decreases exponentially from the initial large value in all the cases. The sum quantity suggests that overall the elastic-inelastic process is favored more at $E_{c.m.} = 9.5$ eV than at $E_{c.m.} = 28.96$ eV and the charge-transfer process is favored almost the same at both energies.

IV. SUMMARY

The comparison of vibronic coupling with earlier work gives us an idea about the quality of computed *ab initio* potential energy values. All the above computed scattering properties show that the present model accounts for the elastic-inelastic process well within the accuracy, whereas this is not so in the case of the charge-transfer channel. The suggestions regarding the improvement of the calculations in order to achieve the agreement with experimental values particularly with the charge-transfer process can be any one or all of the following: (i) change of the basis set, (ii) change of the level of theory suitable to the process under consideration, (iii) change of the method used in the dynamics calculation, (iv) change of the grid parameters in Jacobi coordinates (to finer mesh), (v) change of the electronic states from two to more, possibly three or four, and (vi) change of the modification of the diabaticization procedure. While all of the above options are given on a speculative basis we are of the view that invoking one or more of them may have brought out a reasonable level of agreement between theory and experiment for the case of the charge-transfer process.

ACKNOWLEDGMENTS

One of the authors, F. George D. Xavier, acknowledges the CSIR, New Delhi, for the Senior Research Fellowship. The financial assistance by the IIT Madras in procuring the MOLPRO code through an interdisciplinary research grant in the chemical physics program is also gratefully acknowledged. We thank the IITM for the available computational resources.

TABLE V. Integral cross section compared.

$v(v')$	Integral cross section (\AA^2)			
	9.5 eV		28.96 eV	
	VE	CT	VE	CT
0	69.727	14.715	48.609	14.871
1	2.581	1.021	1.967	1.068
2	0.869	0.372	0.528	0.384
3	0.397	0.217	0.224	0.240
4	0.201	0.145	0.147	0.162
5	0.144	0.117	0.088	0.119
6	0.106	0.111	0.096	0.123
7	0.140	0.098	0.076	0.096
$\sum v(v')$	74.311	17.055	51.735	17.062

- [1] E. Herbst, *Chem. Soc. Rev.* **30**, 168 (2001).
- [2] S. L. Widicus Weaver, D. E. Woon, B. Ruscic, and B. J. McCall, *Astrophys. J.* **697**, 601 (2009).
- [3] H. Udseth, C. F. Giese, and W. R. Gentry, *J. Chem. Phys.* **60**, 3051 (1974).
- [4] V. Hermann, H. Schmidt, and F. Linder, *J. Phys. B* **11**, 493 (1978).
- [5] J. Krutein and F. Linder, *J. Chem. Phys.* **71**, 599 (1979).
- [6] F. A. Gianturco, U. Gierz, and J. P. Toennies, *J. Phys. B: Adv. At. Mol. Phys.* **14**, 667 (1981).
- [7] M. Noll and J. P. Toennies, *J. Chem. Phys.* **85**, 3313 (1986).
- [8] G. Niedner, M. Noll, J. P. Toennies, and C. Schiler, *J. Chem. Phys.* **87**, 2685 (1987).
- [9] G. Niedner-Schatteburg and J. P. Toennies, *Adv. Chem. Phys.* **82**, 553 (1992).
- [10] D. Grimbert, V. Sidis, and M. Sizun, *Chem. Phys. Lett.* **230**, 47 (1994).
- [11] W. Klemperer, *Nature (London)* **227**, 1230 (1970).
- [12] D. Buhl and L. E. Snyder, *Nature (London)* **228**, 267 (1970).
- [13] R. C. Woods, T. A. Dixon, R. J. Saykally, and P. G. Szanto, *Phys. Rev. Lett.* **35**, 1269 (1975).
- [14] P. Botschwina, *Ion and Cluster Ion Spectroscopy and Structure* (Elsevier, Amsterdam, 1989).
- [15] N. L. Ma, B. J. Smith, and L. Radom, *Chem. Phys. Lett.* **197**, 573 (1992).
- [16] J. M. L. Martin, P. R. Taylor, and T. J. Lee, *J. Chem. Phys.* **99**, 286 (1993).
- [17] Y. Yamaguchi, J. C. A. Richards, and H. F. Schaefer III, *J. Chem. Phys.* **101**, 8945 (1994).
- [18] C. Pizzarini, R. Tarroni, P. Palmieri, S. Carter, and L. Dore, *Mol. Phys.* **87**, 879 (1996).
- [19] M. Mladenović and S. Schmatz, *J. Chem. Phys.* **109**, 4456 (1998).
- [20] J. Grunenberg, R. Streubel, G. V. Frantzius, and W. Marten, *J. Chem. Phys.* **119**, 165 (2003).
- [21] A. C. Hopkins, N. K. Holbrook, K. Yates, and I. G. Csizmadia, *J. Chem. Phys.* **49**, 3596 (1968).
- [22] U. Wahlgren, P. K. Pearson, and H. F. Schaefer III, *Nat. Phys. Sci.* **246**, 4 (1973).
- [23] P. J. Bruna, S. D. Peyerimhoff, and R. J. Buenker, *Chem. Phys.* **10**, 323 (1975).
- [24] A. Saieswari and S. Kumar, *Chem. Phys. Lett.* **449**, 358 (2007).
- [25] A. Saieswari and S. Kumar, *J. Chem. Phys.* **127**, 214304(1) (2007).
- [26] A. Saieswari and S. Kumar, *J. Chem. Phys.* **128**, 064301(1) (2008).
- [27] V. Staemmler and F. A. Gianturco, *Int. J. Quantum Chem.* **28**, 553 (1985).
- [28] G. J. Vazquez, R. J. Buenker, and S. D. Peyerimhoff, *Mol. Phys.* **59**, 291 (1986).
- [29] D. Grimbert, B. Lassier-Givers, and V. Sidis, *Chem. Phys.* **124**, 187 (1988).
- [30] F. Schneider, L. Zülicke, F. DiGiacomo, F. A. Gianturco, I. Páidarová, and R. Polák, *Chem. Phys.* **128**, 311 (1988).
- [31] A. Saieswari and S. Kumar, *J. Chem. Phys.* **128**, 154325(1) (2008).
- [32] F. George D. Xavier, *J. Phys. Chem. A* **114**, 10357 (2010).
- [33] F. A. Gianturco, S. Kumar, and F. Schneider, *Chem. Phys.* **211**, 33 (1996).
- [34] F. A. Gianturco, S. Kumar, T. Ritschel, R. Vetter, and L. Zülicke, *J. Chem. Phys.* **107**, 6634 (1997).
- [35] A. Saieswari and S. Kumar, *J. Chem. Phys.* **128**, 124306(1) (2008).
- [36] F. A. Gianturco, U. T. Lamanna, and D. Ignazzi, *Chem. Phys.* **48**, 387 (1980b).
- [37] T. J. Dhilip Kumar and S. Kumar, *J. Chem. Phys.* **121**, 191 (2004).
- [38] T. J. Dhilip Kumar, A. Saieswari, and S. Kumar, *J. Chem. Phys.* **124**, 034314(1) (2006).
- [39] C. Y. Lin, P. C. Stancil, Y. Li, J. P. Gu, H. P. Liebermann, R. J. Buenker, and M. Kimura, *Phys. Rev. A* **76**, 012702(1) (2007).
- [40] M. Kimura, J. P. Gu, G. Hirsch, R. J. Buenker, and P. C. Stancil, *Phys. Rev. A* **61**, 032708(1) (2000).
- [41] C. Y. Lin, P. C. Stancil, Y. Li, J. P. Gu, H. P. Liebermann, R. J. Buenker, and M. Kimura, *Phys. Rev. A* **76**, 012702(1) (2007).
- [42] F. George D. X. and S. Kumar, *J. Chem. Sci.* **119**, 409 (2007).
- [43] F. George D. X. and S. Kumar, *Chem. Phys.* **373**, 211 (2010).
- [44] V. Khare, *J. Chem. Phys.* **67**, 3897 (1977).
- [45] D. J. Kouri, *Atom-Molecule Collision Theory: A Guide for the Experimentalist* (Plenum Press, New York, 1979).
- [46] R. Pack, *J. Chem. Phys.* **60**, 633 (1974).
- [47] G. Parker and R. T. Pack, *J. Chem. Phys.* **68**, 1585 (1978).
- [48] F. A. Gianturco, *The Transfer of Molecular Energies by Collisions* (Springer, Berlin, 1979).
- [49] R. Schinke and P. McGuire, *Chem. Phys.* **31**, 391 (1978).
- [50] R. J. Le Roy, *Chemical Physics Research Report*, Technical Report CP-55R (University of Waterloo, 1996).
- [51] P. H. Krupenie and S. Weissman, *J. Chem. Phys.* **43**, 1529 (1965).
- [52] I. Borges Jr., P. J. S. B. Caridade, and A. J. C. Varandas, *J. Mol. Spectrosc.* **209**, 24 (2001).
- [53] J. T. H. Dunning, *J. Chem. Phys.* **90**, 1007 (1989).
- [54] R. J. Buenker and S. D. Peyerimhoff, *Theor. Chim. Acta* **35**, 33 (1974).
- [55] R. J. Buenker and S. D. Peyerimhoff, *Theor. Chim. Acta* **39**, 217 (1975).
- [56] R. J. Buenker and R. A. Philips, *THEOCHEM* **123**, 291 (1985).
- [57] S. Krebs and R. J. Buenker, *J. Chem. Phys.* **103**, 5613 (1995).
- [58] H.-J. Werner and P. J. Knowles, *J. Chem. Phys.* **89**, 5803 (1988).
- [59] P. J. Knowles and H.-J. Werner, *Chem. Phys. Lett.* **145**, 514 (1988).
- [60] P. J. Knowles and H.-J. Werner, *Theor. Chim. Acta* **84**, 95 (1992).
- [61] M. Baer, G. Niedner-Schatteburg, and J. P. Toennies, *J. Chem. Phys.* **91**, 4182 (1989).
- [62] N. P. F. B. van Asselt, J. G. Maas, and J. Los, *Chem. Phys.* **16**, 81 (1976).
- [63] M. R. Spalburg and J. Los, *Chem. Phys.* **103**, 253 (1986).